



Axial strength and ductility of square composite columns with two interlocking spirals



Tsu-Han Shih^a, Cheng-Chih Chen^{a,*}, Cheng-Chiang Weng^a, Samuel Yen-Liang Yin^b, Jui-Chen Wang^b

^a Department of Civil Engineering, National Chiao Tung University, 1001 University Road, Hsinchu, 300, Taiwan

^b Ruentex Group, 14F, No. 308, Sec. 2, Bade Road, Taipei, 104, Taiwan

ARTICLE INFO

Article history:

Received 18 March 2013

Accepted 20 July 2013

Available online 4 September 2013

Keywords:

Composite column

Spiral

Axial compression

Strength

Ductility

ABSTRACT

The axial compressive capacity and load–displacement behaviour of composite columns confined by two interlocking spirals were experimentally and analytically investigated. The innovative spiral cage used for a square column was fabricated by interlocking a circular spiral and a star-shaped spiral to enhance the confinement effect for the core concrete. Eight full-scale square composite columns were tested under monotonically increased axial compression. Experimental results demonstrated that, with significant savings of the transverse reinforcement, the composite columns confined by two interlocking spirals achieved excellent axial compressive strength and ductility capacity. Moreover, an analytical model was developed to take into account the concrete confinement due to the structural steel in addition to the transverse reinforcement and distributions of the longitudinal bars. The analytical results accurately predicted the axial compressive capacity and load–displacement behaviour of the specimens. Consequently, the application of the two interlocking spirals in a square composite column appears to be very affirmative.

© 2013 Elsevier Ltd. All rights reserved.

1. Introduction

Various experimental and numerical studies have shown that transverse reinforcement in columns functions as follows: (1) holding longitudinal bars in position; (2) preventing longitudinal bars from premature buckling; (3) providing shear strength for columns; (4) providing passive confinement for core concrete; and (5) improving axial compressive strength and ductility of columns [1–7]. Square columns are traditionally reinforced with rectangular hoops, and each hoop is formed from a single steel bar with hook at both ends [8]. However, field experiences reveal that hoops with a 135-degree bend are difficult to setup in a composite column, and the entire construction is heavily relied on skilled labors that is time-consuming and costly.

Spirals are a continuously wound transverse reinforcement and can be fabricated automatically in a factory. The fabrication of helical spirals is faster and cheaper than that of rectilinear hoops. Moreover, helical spirals in a column are more effective in providing concrete confinement compared to rectilinear hoops [9,10]. Mirza and Skrabek [11,12] studied the behaviour of short and slender composite columns subjected to axial force and bending moment. Ricles and Paboojian [13] investigated the seismic behaviour of composite columns through experiments. They concluded that the strength and toughness of composite columns were affected by the confinement status of the core concrete. Exactly how the spirals apply to columns with square cross section is of interest. Fig. 1(a) shows a square column reinforced by a circular helical spiral.

Because the concrete at the four corners of the square column cannot be confined by the circular spiral, applications of the circular spiral to square columns are not common in engineering practice.

This research proposes an innovative spiral confinement as shown in Fig. 1(b). The confinement is achieved by two interlocking spirals, consisting of a circular spiral and a star-shaped spiral, with longitudinal bars located around the perimeter of the square column. The interlocking spirals overcome the shortcomings of applications of a circular spiral to square cross-sectional columns, and facilitate sound confinement for the concrete at the four corners of the square column. Moreover, the manpower and construction time to fabricate reinforcement cage can be substantially reduced because the spirals can be fabricated by automatic machines in the factory. Fig. 2 illustrates the construction of the two interlocking spirals.

This work elucidates experimentally and analytically the effectiveness of the two interlocking spirals used in square composite columns. Eight full-scale columns, including six spirally reinforced composite columns and two reinforced concrete columns, were tested under monotonically increased axial compression. An analytical approach was also conducted to calculate the axial compressive strength and the load–deformation relationships of the specimens.

2. Experimental program

2.1. Design of test specimens

Table 1 presents the details of the specimens. Six of the specimens (SRC1 ~ 6) were composite columns reinforced with two spirals. The

* Corresponding author. Tel.: +886 3 571 2121x54915; fax: +886 3 572 7109.
E-mail address: chrischen@mail.nctu.edu.tw (C.-C. Chen).

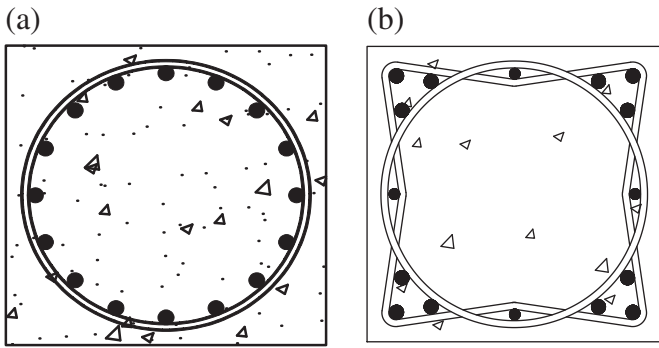


Fig. 1. Spiral confinements for a square column: (a) a circular spiral; (b) two interlocking spirals.

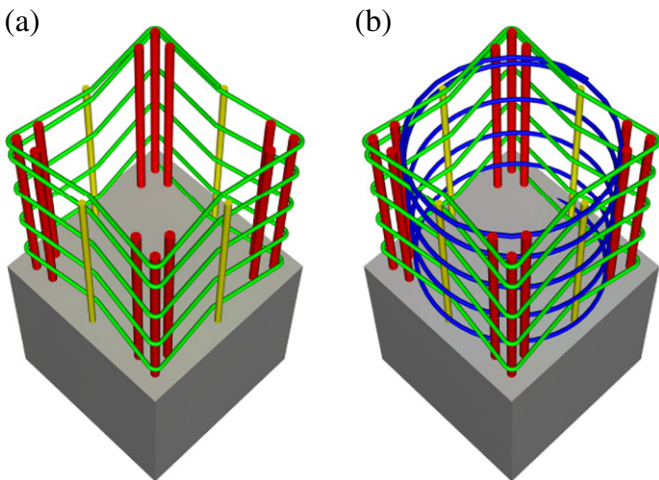
other two specimens (RC1 and RC2) were reinforced concrete columns with rectilinear hoops. The test specimens were 600 mm square in the cross section and 1200 mm long. Two types of structural steel sections used were welded built-up box section (□250 × 250 × 6 × 6 and □300 × 300 × 9 × 9) and cross-H section (2-H220 × 100 × 6 × 9 and 2-H350 × 175 × 6 × 9). The ratios of the area of structural steel section to gross section of the column are presented in the table.

Regarding the design of the transverse reinforcement, different design specifications were considered, including ACI 318 building code [8] and AISC seismic provisions [14]. Specimen RC2, served as the benchmark, was designed to have minimum rectilinear hoops according to ACI 318 building code.

$$A_{sh} = 0.3sh_c \frac{f'_c}{f_{yt}} \left(\frac{A_g}{A_{ch}} - 1 \right) \quad (1a)$$

$$A_{sh} = 0.09sh_c \frac{f'_c}{f_{yt}} \quad (1b)$$

where A_{sh} is the total cross-sectional area of hoop reinforcement within spacing s ; A_g and A_{ch} are the gross cross-sectional area of the column and the cross-sectional area measured to outside edges of hoop reinforcement, respectively; f'_c is the specified compressive strength of concrete; f_{yt} is the specified yield strength of hoop reinforcement; s is the center-to-center spacing of hoop reinforcement; and h_c is the width of confined core concrete.



(Structural steel not shown for clarity)

Fig. 2. Construction of the two interlocking spirals: (a) fabricated cage of the star-shaped spiral; (b) insert of the circular spiral.

For the spirally reinforced concrete column, specimen RC1, ACI 318 building code stipulates that the volumetric ratio, ρ_s , defined as the ratio of the volume of spiral reinforcement to the volume of core concrete, shall not be less than the following requirement:

$$\rho_s = 0.45 \frac{f'_c}{f_{yt}} \left(\frac{A_g}{A_{ch}} - 1 \right) \quad (2a)$$

$$\rho_s = 0.12 \frac{f'_c}{f_{yt}} \quad (2b)$$

Regarding the transverse reinforcement used in composite columns, AISC seismic provisions propose a formula based on ACI 318 building code. A reduction factor of $(1 - f_{ys}A_s/P_n)$ is used to reduce the requirement for the tie reinforcement to take into account the structural steel core. The minimum tie reinforcement shall meet the following:

$$A_{sh} = 0.09sh_c \frac{f'_c}{f_{yt}} \left(1 - \frac{f_{ys}A_s}{P_n} \right) \quad (3)$$

in which A_s and f_{ys} are the cross-sectional area and specified yield strength of the structural steel, respectively; P_n is the nominal axial compressive strength of the composite column calculated in accordance with the AISC specification [15]. Hence, for designing the spirally reinforced composite columns, specimens SRC1 ~ 3, a formula adopting a reduction factor according to the same design philosophy is proposed as follows.

$$\rho_s = 0.45 \frac{f'_c}{f_{yt}} \left(\frac{A_g}{A_{ch}} - 1 \right) \left(1 - \frac{f_{ys}A_s}{P_n} \right) \quad (4)$$

Moreover, in recognition for the superior confinement provided by the structural steel section in composite columns [12,16], as indicated in Fig. 3, Weng et al. [17] proposed a formula to account for reducing transverse reinforcement due to the highly confined concrete in composite columns. The following equation was used to design the required spirals for specimens SRC4 ~ 6.

$$\rho_s = 0.45 \frac{f'_c}{f_{yt}} \left(\frac{A_g}{A_{ch}} - 1 \right) \left(1 - \frac{P_s + P_{hcc}}{P_o} \right) \quad (5a)$$

where

$$P_o = f_{ys}A_s + f_{yt}A_r + 0.85f'_cA_c \quad (5b)$$

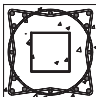
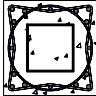
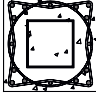

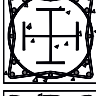
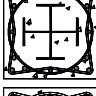


$$P_s = f_{ys}A_s \quad (5c)$$

$$P_{hcc} = 0.85f'_cA_{hc} \quad (5d)$$

where P_o is the nominal axial compressive strength of the composite column; P_s and P_{hcc} are the compressive strength provided by the structural steel and highly confined concrete, respectively; f_{yt} is the specified yield strength of the longitudinal reinforcement; A_r is the cross-sectional area of the longitudinal reinforcement; A_c is the cross-sectional area of the concrete section; and A_{hc} is the area of highly confined concrete.

Accordingly, the use of the transverse reinforcement for each specimen is shown in Table 1. Besides, the weights of the transverse reinforcement per unit length of the column are also presented. On the basis of the reduction for the transverse reinforcement specified in Eqs. (4) and (5), composite columns (specimens SRC1 ~ SRC6) utilized less transverse reinforcement compared to the reinforced concrete columns (specimens RC1 and RC2). Fig. 4 depicts the details of the cross section of specimen SRC2, confined by two interlocking spirals.

Table 1
Details of the specimens.

Specimen designation	Structural steel		Longitudinal bar		Transverse reinforcement				Weight of transverse reinf. (N/m of col.)	Cross section
	Size (mm)	Area ratio	Size	Area ratio	Circular spiral	Star-shaped spiral	Rectilinear hoop	Spacing (mm)		
SRC1	□250 × 250 × 6 × 6	1.63%	12 No.8	1.69%	No. 4	No. 4	-	115	325	
SRC2	□300 × 300 × 9 × 9	2.91%	12 No.8	1.69%	No. 4	No. 4	-	130	286	
SRC3	□300 × 300 × 9 × 9	2.91%	12 No.8	1.69%	No. 4	No. 3	-	100	282	
SRC4	Two H220 × 100 × 6 × 9	1.66%	12 No.8	1.69%	No. 4	No. 4	-	125	298	
SRC5	Two H350 × 175 × 6 × 9	2.91%	12 No.8	1.69%	No. 4	No. 4	-	150	248	
SRC6	Two H350 × 175 × 6 × 9	2.91%	12 No.8	1.69%	No. 4	No. 3	-	125	226	
RC1	-	-	8 No.10 8 No.11	4.05%	No. 4	No. 4	-	100	376	
RC2	-	-	8 No.10 8 No.11	4.05%	-	-	No. 4	90	405	

2.2. Material properties

Ready-mix normal weight concrete was used for the specimens and standard cylinders of 150 × 300 mm were cast also. ASTM C39/C39M [18] test procedures were followed to determine the concrete compressive strength. Because concrete strength is highly depended on the curing condition, the compressive strength of the cylinders cured in the same condition as the columns was used. The average compressive strength of three cylinders was 32.3 MPa measured at the time of testing.

The steel plates used for the structural steel core were all A572 Gr. 50 steel. All the longitudinal bars and circular spirals were ASTM A615 [19] Gr. 60 deformed bars. Owing to fabrication requirement, star-shaped spirals were deformed wires confirming ASTM A496 [20]. Three coupons were cut from each steel material and were tested in accordance with ASTM A370 [21] to obtain the yield and ultimate strengths.

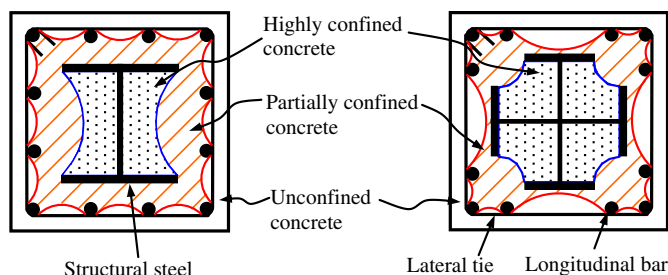


Fig. 3. Concrete confinement in composite columns.

Table 2 presents the average material properties of the steel plates, deformed bars, and deformed wires. Instead of the specific strengths, the measured material strengths were adopted to evaluate the performance of the specimens.

2.3. Test setup

Fig. 5 shows the setup of the axial compression test for the specimens. A 58,800 kN hydraulic jack applied compressive force at a constant stroke rate of 0.03 mm/s. To achieve a uniform load distribution on the specimens, end caps were mounted on both column ends. Extensometers of linear variable differential transformers were installed to measure the axial shortening of the specimens.

3. Experimental results and discussions

3.1. General behaviour and failure mode

All specimens demonstrated similar global behaviour. Before cracks were observed on the concrete surface, specimens exhibited linear elastic behaviour. Minor longitudinal cracks gradually appeared on the concrete surface, and these cracks propagated longitudinally while the axial compressive force was increased continuously. Caused by the serious cracking, concrete cover began to spall when the specimens reached their ultimate strengths. Post-peak behaviours of the specimens were massive spalling of the concrete cover, buckling of the longitudinal bars, and rupturing of the spirals or hoops.

Fig. 6 shows the failure appearance of specimens RC2, SRC2, and SRC3 after removing the spalled concrete cover. As indicated in Fig. 6(a), the

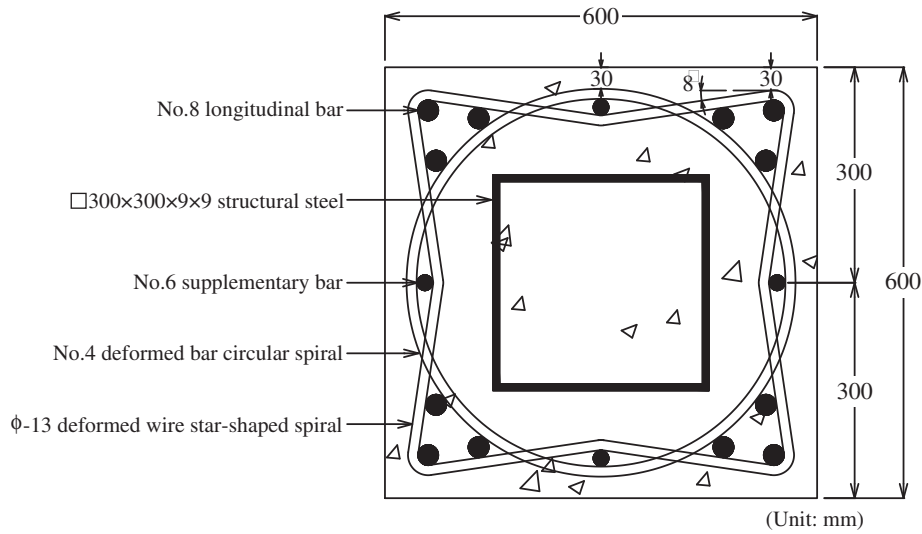


Fig. 4. Cross section of spirally reinforced composite column, specimen SRC2.

rectilinear hoop in specimen RC2 ruptured at the hook. The circular spiral of specimen SRC2, having No. 4 circular and star-shaped spirals, ruptured as presented in Fig. 6(b); however, the star-shaped spiral was not damaged. As a result, the star-shaped spiral could still confine the core concrete and prevent buckling of the longitudinal bars located at the corner of the column. Specimen SRC3 was designed to have No. 4 circular spiral and No. 3 star-shaped spiral. Because of the smaller size, the star-shaped spiral ruptured but the circular spiral was undamaged as shown in Fig. 6(c). The rupture of the star-shaped spiral led to severe buckling of the longitudinal bars at the corner of the column, and, consequently, the axial compressive strength of the specimen deteriorated.

Fig. 7 depicts the axial compressive strength versus axial displacement relations of the specimens. The test axial compressive strength was normalized by dividing the squash strength, P_{squash} . The squash strength was calculated the same as P_o in Eq. (5b) but the measured material strengths tabulated in Table 2 were used. The two interlocking spirals could provide confinement to the core concrete and prevent buckling of the longitudinal bars, and then the confinement resulted in the increase of the axial compressive strength that can be observed from Fig. 7. Moreover, the spirally reinforced composite columns exhibited gentle descending branch at the load–displacement curve.

3.2. Axial compressive strength and ductility

Table 3 tabulates the maximum test axial compressive strengths, P_{test} , and squash strengths, P_{squash} , for all specimens. Squash strengths of the columns represent the sum of all the axial compressive strengths

contributed from each structural material, based on the assumption of strain compatibility. Thus, the increase of the axial compressive strength due to concrete confinement was not considered. Therefore, the strength ratio of P_{test} to P_{squash} implied degree of the concrete confinement effect. As shown in Table 1, specimens RC1 (two interlocking spirals) and RC2 (rectilinear hoops) had the same amount of the longitudinal bars; however, specimen RC1 had fewer amount of the transverse reinforcement than specimen RC2. Specimen RC1 attained 9% higher axial compressive strength than specimen RC2 because of the great confinement effect provided by the two interlocking spirals.

Specimens SRC1 and SRC4 had lower structural steel ratio (1.63% and 1.66%, respectively) than other specimens (2.91%). The strength ratios of these two specimens were approximately the same as that of specimen RC1. Nevertheless, all other composite column specimens with higher steel ratio attained higher strength ratio than specimen RC1 that implied the structural steel shape could provide superior confinement to the core concrete.

To evaluate the ductility capacity of the specimens, a ductility index was defined as the ratio of the post-peak displacement corresponding to 70% of the peak load, $\delta_{0.7P_u}$, to the displacement corresponding to the peak load, δ_{P_u} . The larger the ductility index, the better seismic performance of the column. As presented in Table 3, spirally reinforced concrete column (specimen RC1) had better ductility capacity than rectilinearly tied reinforced concrete column (specimen RC2). Furthermore, because the structural steel shape enhanced the confinement for the core concrete, spirally reinforced composite columns, specimens SRC1 ~ SRC6 having ductility indices ranging from 5.03 to 8.67, attained much better ductility capacity than reinforced concrete columns, specimens RC1 and RC2 having ductility indices of 4.08 and 3.73, respectively. Cyclic behaviour is one of the most important issues while the columns are subjected to seismic load. The future research is needed to investigate seismic performance of the composite columns with two interlocking spirals.

3.3. Effect of the transverse reinforcement

Since the circular and star-shaped spirals are interlocking, the circular spiral has a crosstie-like effect over the star-shaped spiral through the use of the longitudinal bars. When the specimens were subjected to the axial compression, the circular spiral not only confined the concrete but also suppressed the lateral deformation of the star-shaped spiral. The circular spiral functioned as a crosstie to improve the performance of the star-shaped spiral. The two interlocking spirals

Table 2
Measured strengths of steel materials used in the specimens.

	Steel plate thickness (mm)		Reinforcing bar					
	6	9	Deformed wire		Deformed bar			
			No. 3	No. 4	No. 4	No. 8	No. 10	No. 11
Yield strength (MPa)	421	386	552	525	463	469	452	530
Ultimate strength (MPa)	571	529	635	601	707	658	705	756

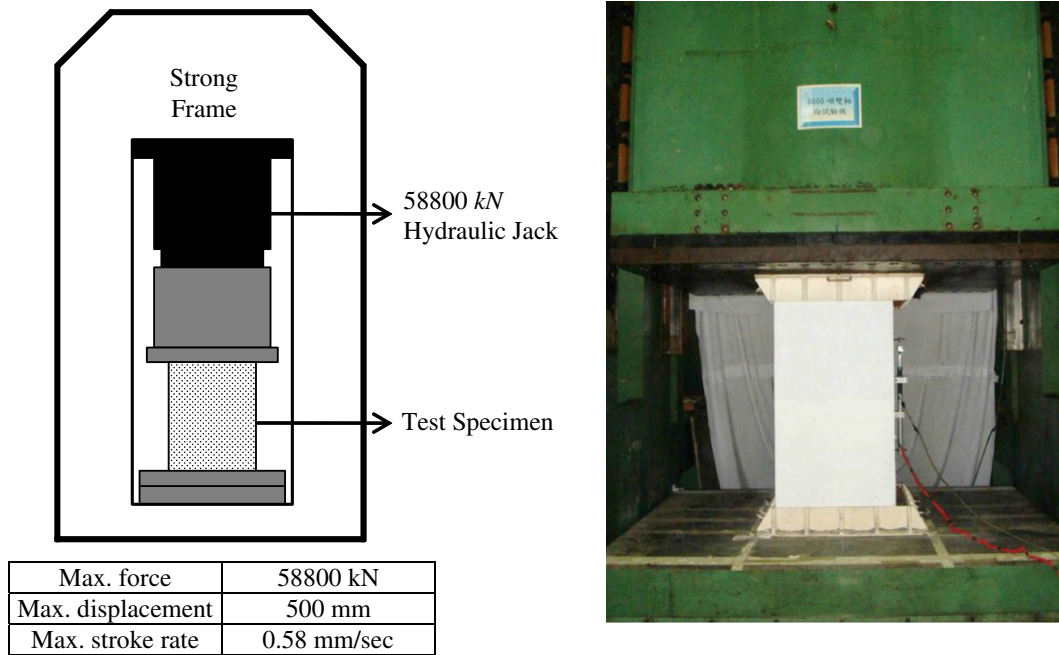


Fig. 5. The 58,800 kN test machine and the test setup.

simultaneously confined the core concrete and prevented the premature buckling of the corner longitudinal bars. Therefore, the two interlocking spirals increased the axial compressive strength and the ductility of the columns.

Table 1 tabulates also the weights of the transverse reinforcement per unit length of the column used in the specimens. Spirally reinforced concrete specimen RC1 used less transverse reinforcement than rectilinearly tied reinforced concrete specimen RC2, but specimen RC1 developed better strength ratio and ductility capacity than specimen RC2. All composite specimens used less transverse reinforcement than RC columns. However, the spirally reinforced composite columns not only exhibited adequate strength and ductility performance but also confirmed satisfactory economic benefit, especially for specimens SRC5 and SRC6.

4. Analytical prediction

4.1. Analytical modeling

An analytical approach was conducted to predict the axial compressive strength and load–displacement behaviour of the specimens. The cross section of a composite column can be divided into several areas as shown in Fig. 8. The confined concrete in a composite column is different from that in a reinforced concrete column. The concrete in composite column was assumed to be categorized into four different areas: (1) a highly confined area that concrete confined simultaneously by the structural steel, circular spiral, and star-shaped spiral; (2) a doubly confined area that concrete confined by the circular and star-shaped spirals; (3) a singly confined area that concrete confined by either the

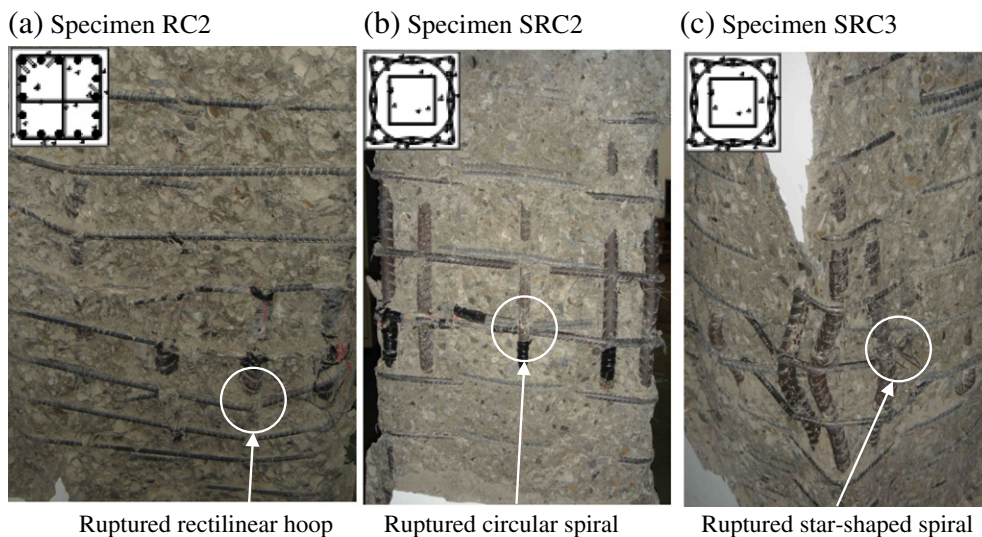


Fig. 6. Failure appearance of specimens after removing the spalled concrete cover.

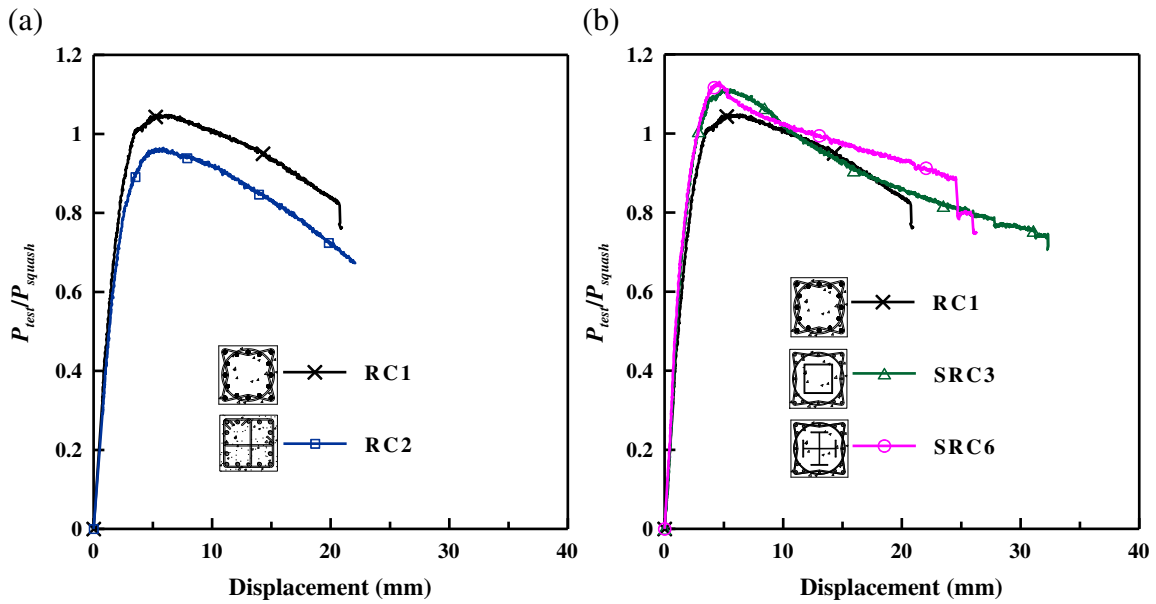


Fig. 7. Normalized load–displacement curves of RC and composite columns.

Table 3
Experimental results.

Specimen	Axial strength		Strength ratio $\frac{P_{test}}{P_{squash}}$	Axial displacement		Ductility index $\frac{\delta_{0.7P_u}}{\delta_{P_u}}$
	P_{test} (kN)	P_{squash} (kN)		δ_{P_u} (mm)	$\delta_{0.7P_u}$ (mm)	
SRC1	15,559	14,865	1.05	3.18	21.61	6.80
SRC2	17,913	16,316	1.10	3.58	24.63	6.88
SRC3	18,139	16,316	1.11	5.54	27.84	5.03
SRC4	15,323	14,805	1.04	4.51	30.69	6.80
SRC5	18,541	16,496	1.12	3.47	30.07	8.67
SRC6	18,639	16,496	1.13	4.62	25.93	5.61
RC1	17,501	16,700	1.05	5.22	21.31	4.08
RC2	16,108	16,700	0.96	5.88	21.91	3.73

circular spiral or star-shaped spiral; and (4) an unconfined area that concrete located outside the transverse reinforcement. In accordance with the stress–strain models of the different materials, the analytical axial compressive strength and load–displacement curve were calculated by summing the strengths contributed from each material. The stress–strain relations of various materials used in the spirally reinforced composite columns are briefly presented herein.

A widely accepted stress–strain model proposed by Mander et al. [5] was used to establish the stress–strain relations of the confined concrete as follows.

$$f_c = \frac{f'_{cc} \chi r}{r - 1 + \chi^r} \tag{6a}$$

with

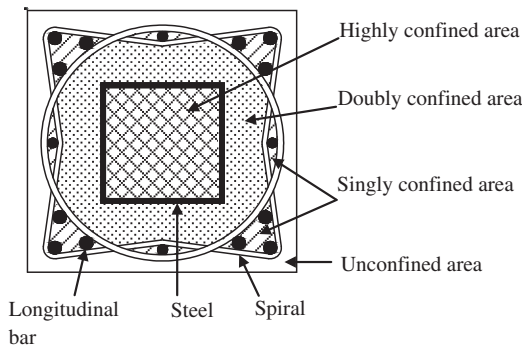
$$\chi = \frac{\epsilon_c}{\epsilon_{cc}} \tag{6b}$$

$$r = \frac{E_c}{E_c - E_{sec}} \tag{6c}$$

$$f'_{cc} = f'_{co} \left(-1.254 + 2.254 \sqrt{1 + \frac{7.94 f'_l}{f'_{co}} - 2 \frac{f'_l}{f'_{co}}} \right) \tag{6d}$$

$$K = -1.254 + 2.254 \sqrt{1 + \frac{7.94 f'_l}{f'_{co}} - 2 \frac{f'_l}{f'_{co}}} \tag{6e}$$

(a) Box section structural steel



(b) Cross-H section structural steel

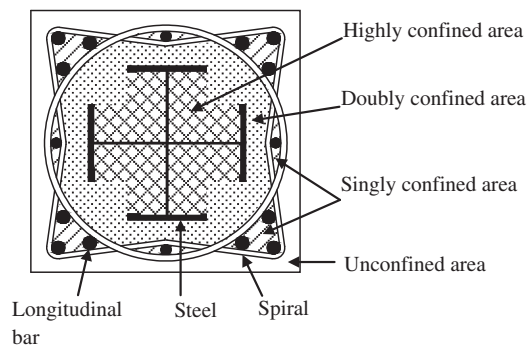


Fig. 8. Concrete confinement areas of the composite columns.

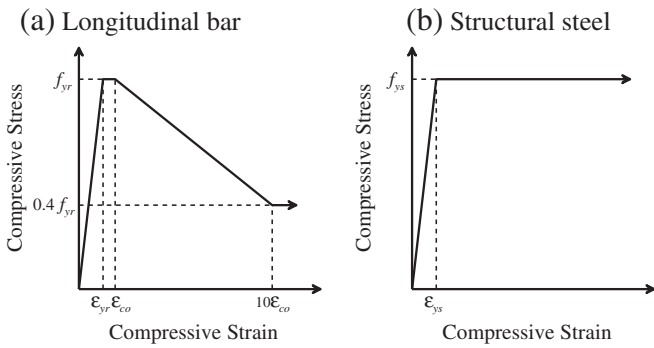


Fig. 9. Stress–strain curves used for longitudinal bar and structural steel.

$$\varepsilon_{cc} = \varepsilon_{co} \left[1 + 5 \left(\frac{f'_{cc}}{f'_{co}} - 1 \right) \right] \quad (6f)$$

where f'_{cc} and ε_{cc} are the maximum compressive stress and the corresponding strain of the confined concrete, respectively; E_c is the tangent modulus of elasticity of the concrete; E_{sec} is the secant modulus of the confined concrete at peak stress; f'_{co} and ε_{co} are the unconfined concrete compressive strength and the corresponding strain, respectively; f'_i is the effective lateral confining stress; and K is the confinement factor for confined concrete.

The stress–strain relations modeled for the longitudinal bar were assumed that the longitudinal bar would buckle when the concrete cover spalled. Therefore, when the axial compressive strain exceeded the strain ε_{co} , corresponding to the unconfined concrete compressive strength f'_{co} , the strength of the longitudinal bar gradually dropped to 40% of its yield strength and maintained constant after the axial strain reached ten times of the strain ε_{co} , as shown in Fig. 9(a). The ten times of the strain ε_{co} was assumed based on that the axial compressive strength of the double-spirally reinforced composite specimens was characterized by a slow decrease at the descending branch of the load–displacement curve as shown in the experiments.

The embedded structural steel effectively confined by the core concrete because the core concrete remained undamaged until the end of the experiment. As a result, the local buckling of the structural steel did not occur; thus, a linearly elastic–perfectly plastic stress–strain curve without any strength degradation was adopted for the structural steel, as shown in Fig. 9(b).

4.2. Analytical results

The concrete confinement factor K is mainly affected by the effective lateral confining stress f'_i . At the highly confined concrete area, the lateral confining stress was enhanced by the structural steel section in addition to the transverse reinforcement. Elements of the structural steel section were considered to calculate the confining stress. Different confinement factors were determined based on the category of the confined concrete via Eq. (6e) suggested by Mander et al.

Table 4 tabulates the calculated confinement factors K_s , K_d and K_h for singly, doubly and highly confined concrete, respectively. The confinement factor K_s for singly confined concrete is highly affected by the spacing of either the circular or star-shaped spiral, and the distribution of the longitudinal bars. Next, the confinement factor K_d for doubly confined concrete is influenced by both the circular and star-shaped spirals in addition to the longitudinal bars. The confinement factor K_h for highly confined concrete is greatly dependent on the structural steel section. As a result, the confinement factor K_h is the greatest among the confinement factors while the confinement factor K_s is the smallest one, as evidenced in Table 4. Moreover, the confinement factors K_h of specimens SRC1 and SRC4, with smaller structural steel section than other

Table 4 Analytical modeling and comparison between experimental and analytical results.

Specimen	Cross-sectional area (mm ²)		Concrete confinement factor										Compressive strength (kN)		
	Structural steel	Longit. bar	Unconfined concrete	Singly confined concrete, hoop	Singly confined concrete, circular	Singly confined concrete, star-shaped	Doubly confined concrete	Highly confined concrete	Singly confined, hoop	Singly confined, circular	Singly confined, star-shaped	Doubly confined	Highly confined	Test	Analysis
	A_s	A_y	A_{uc}	$A_{s,hoop}$	$A_{s,circular}$	$A_{s,star}$	A_{dc}	A_{hc}	$K_{s,hoop}$	$K_{s,circular}$	$K_{s,star}$	K_d	K_h	P_{test}	$P_{analysis}$
SRC1	5856	6080	102,751	-	18,719	33,869	136,081	56,644	-	1.241	1.204	1.330	1.512	15,559	16,193
SRC2	10,476	6080	102,751	-	18,719	33,869	108,581	79,524	-	1.212	1.176	1.286	1.825	17,913	17,856
SRC3	10,476	6080	99,456	-	17,263	37,165	110,036	79,524	-	1.278	1.150	1.301	1.811	18,139	17,902
SRC4	5988	6080	102,751	-	18,719	33,869	164,581	28,012	-	1.221	1.185	1.300	1.363	15,323	15,908
SRC5	10,248	6080	102,751	-	18,719	33,869	106,706	81,627	-	1.182	1.147	1.239	1.583	18,541	17,590
SRC6	10,248	6080	99,456	-	17,263	37,165	108,161	81,627	-	1.221	1.115	1.232	1.563	18,639	17,567
RC1	-	14,597	106,756	-	28,664	31,912	178,070	-	-	1.290	1.294	1.321	-	17,501	17,800
RC2	-	14,597	102,647	242,756	-	-	-	-	1.312	-	-	-	-	16,108	16,408
														Average	1.003
														Coefficient of variation	0.036

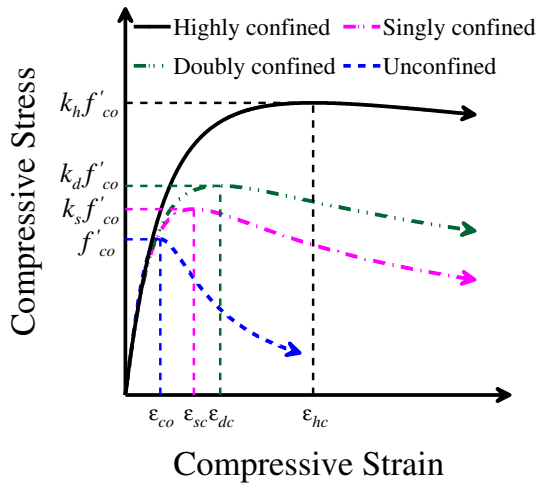


Fig. 10. Compressive stress–strain curve of confined concrete based on different confinement factors.

composite specimens, are considerably lower than those of other specimens.

Calculated according to the equations mentioned before, the compressive stress–strain curves for various confined concrete are illustrated in Fig. 10. The confinement factors mainly influenced the ultimate strength and post-peak behaviour of the confined concrete.

On the basis of strain compatibility, the load–displacement curves for the specimens were calculated at a given axial compressive strain ϵ . The analytic compressive strength $P_{analysis}$ was determined as follows.

$$P_{analysis} = f_s A_s + f_r A_r + f_{uc} A_{uc} + f_{sc,circular} A_{sc,circular} + f_{sc,star} A_{sc,star} + f_{dc} A_{dc} + f_{hc} A_{hc} \quad (15)$$

where the definitions for the areas are shown in Table 4; and the variables of f are the stresses corresponding to the areas.

Fig. 11 illustrates the analytical and experimental load–strain curves of specimens SRC2 and SRC5. A good agreement between the analytical and experimental load–strain relationships is obtained at both pre-peak and post-peak behaviour. Table 4 summarizes the maximum axial compressive strengths of the experiments and

analyses for all the specimens. The analytical predictions are very close to the experimental results. The ratios of the experimental to analytical strength, $P_{test}/P_{analysis}$, range from 0.961 to 1.061. The average ratio is 1.003 and the coefficient of variation is 0.036. Moreover, the analytical approach is more accurate to predict the maximum test strengths than the calculated squash strengths because the squash strengths did not take into account the confinement effect of the core concrete.

5. Conclusions

Six full-scale composite columns and two reinforced concrete columns were tested under axial compression. An analytical approach was developed to predict axial compressive strengths and behaviour of the specimens. Based on the experimental and analytical results, the following conclusions can be drawn.

1. The experimental results revealed that the spirally reinforced concrete column achieved better load-carrying capacity and behaviour than the rectilinearly tied reinforced concrete column, although the amount of the spirals was less than that of the rectilinear hoops.
2. Compared to the spirally reinforced concrete column, the spirally reinforced composite columns demonstrated excellent axial strength and ductility performance attributed to the confinement resulting from structural steel.
3. The spirally reinforced composite columns with larger structural steel resulted in higher axial strength ratio because the structural steel provided superior confinement to the core concrete.
4. In general, experimental results have demonstrated the advantages in strength and ductility improvement as well as economic benefit increment in applying the two interlocking spirals to square composite columns.
5. The analytical results exhibited that the analytical model can accurately predict not only the axial compressive strength but also the load–displacement relations of the spirally confined composite columns.

Acknowledgments

The authors would like to thank the Ruentex Engineering & Construction Co., Ltd. of Taiwan, for financially supporting this research.

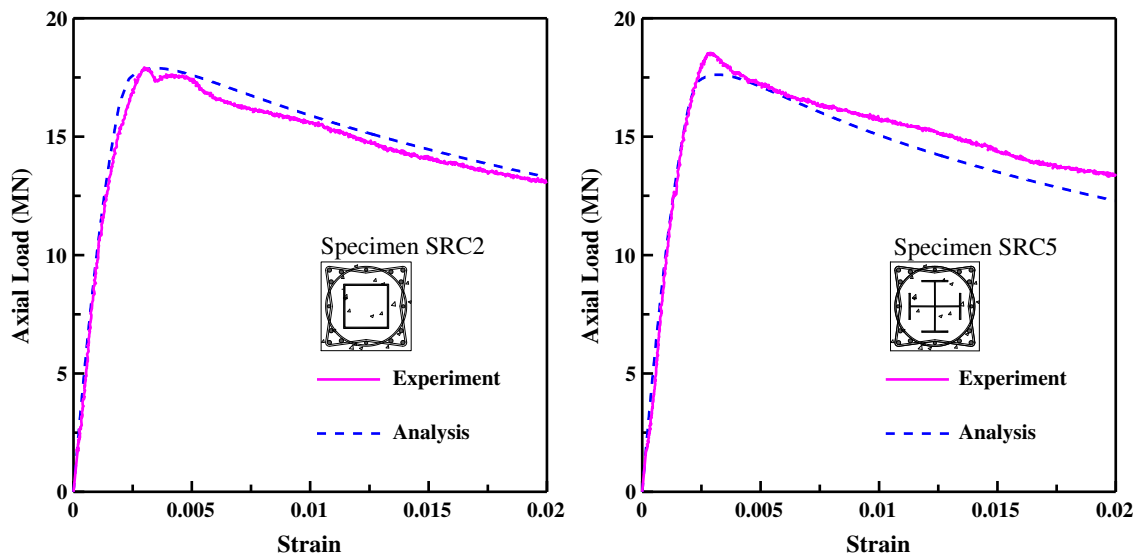


Fig. 11. Analytical and experimental load–strain curves of specimens SRC2 and SRC5.

References

- [1] King JWH. The effect of lateral reinforcement in reinforced concrete columns. *Struct Eng* 1946;24(7):355–88.
- [2] Darwin D, Pecknold DA. Nonlinear biaxial stress-strain law for concrete. *J Eng Mech Div ASCE* 1977;103(2):229–41.
- [3] Sheikh SA, Uzumeri SM. Analytical model for concrete confinement in tied columns. *J Struct Div ASCE* 1982;108(12):2703–22.
- [4] Moehle JP, Cavanagh T. Confinement effectiveness of crosstie in RC. *J Struct Eng ASCE* 1985;111(10):2105–20.
- [5] Mander JB, Priestly MJN, Park R. Theoretical stress-strain model for confined concrete. *J Struct Eng ASCE* 1988;114(8):1804–26.
- [6] Saatcioglu M, Razvi SR. Strength and ductility of confined concrete. *J Struct Eng ASCE* 1992;118(6):1590–607.
- [7] Pantazopoulou SJ. Detailing for reinforcement stability in RC members. *J Struct Eng ASCE* 1998;124(6):623–32.
- [8] ACI Committee 318. Buildings code requirements for structural concrete (ACI 318-08) and commentary. American Concrete Institute; 2008.
- [9] Shah SP, Fafitis A, Arnold R. Cyclic loading of spirally reinforced concrete. *J Struct Eng ASCE* 1983;109(7):1695–710.
- [10] Sheikh SA, Toklucu MT. Reinforced concrete columns confined by circular spirals and hoops. *ACI Struct J* 1993;90(5):542–53.
- [11] Mirza SA, Skrabek BW. Reliability of short composite beam-column strength interaction. *J Struct Eng ASCE* 1991;117(8):2320–39.
- [12] Mirza SA, Skrabek BW. Statistical analysis of slender composite beam-column strength. *J Struct Eng ASCE* 1992;118(5):1312–32.
- [13] Ricles JM, Paboojian SD. Seismic performance of steel encased composite columns. *J Struct Eng ASCE* 1994;120(8):2474–94.
- [14] AISC. Seismic provisions for structural steel buildings. American Institute of Steel Construction; 2005.
- [15] AISC. Specification for structural steel buildings. American Institute of Steel Construction; 2005.
- [16] Li L, Sakai J, Matsui C. Seismic behavior of steel encased reinforced concrete beam-columns. Proceedings of the international conference on advances in structures; 2003. p. 1201–7.
- [17] Weng CC, Yin YL, Wang JC, Liang CY. Seismic cyclic loading test of SRC columns confined with 5-spirals. *Science in China Series E. Technological Sciences* 2008;51(5):529–55.
- [18] ASTM C39/C39M. Standard test method for compressive strength of cylindrical concrete specimens. ASTM International; 2005.
- [19] ASTM A615/A615M. Standard specification for deformed and plain billet-steel bars for concrete reinforcement. ASTM International; 2005.
- [20] ASTM A496/A496M. Standard specification for steel wire, deformed, for concrete reinforcement. ASTM International; 2005.
- [21] ASTM A370. Standard test methods and definitions for mechanical testing of steel products. ASTM International; 2005.